Optimal Configuration of a Planet-Finding Mission Consisting of a Telescope and a Constellation of Occulters

Egemen Kolemen* and N. Jeremy Kasdin *
Princeton University, Princeton, NJ, 08544, USA

The optimal configuration of satellite formations consisting of a telescope and multiple occulters around Sun-Earth L2 Halo orbits is studied. Focusing on the Quasi-Halo orbits, which are of interest for occulter placement, the phase space around L2 is examined. Trajectory optimization of the occulter motion between imaging sessions of different stars is performed. This enables the transformation of the global optimization problem into a Time-Dependent Traveling Salesman Problem (TSP). First, the TSP is solved for a simpler formation consisting of a telescope and a single occulter. Using dynamical insight around L2, approximate initialization regions of the occulter formation are identified. Combining the initialization and the methods developed for single occulter formation, a solution to the full TSP is obtained, which will enable a trade-off study of multiple occulters in terms of cost and scientific achievement.

I. Introduction

It is likely that the next decade will see NASA launch the first in a series of missions dubbed the Terrestrial Planet Finders (TPF) to detect, image, and characterize extrasolar earthlike planets. Current work is directed at studying a variety of architecture concepts and the associated optical engineering in order to prove the feasibility of such a mission. One such concept involves the formation flying of a conventional space telescope on the order of 2 to 4 meter diameter, in a Sun-Earth L2 Halo orbit, with multiple large occulters, roughly 30 m across and 50,000 km away, to block the light of a star and allow imaging of its dim, close-by planetary companion. Recent results in shaped-pupil technology at Princeton have made the manufacture of such a starshade feasible.[1,2] This approach to planet imaging eliminates all of the precision optical requirements that exist in the alternate coronagraphic or interferometric approaches. However, it introduces the difficult problem of controlling and realigning the satellite formation.

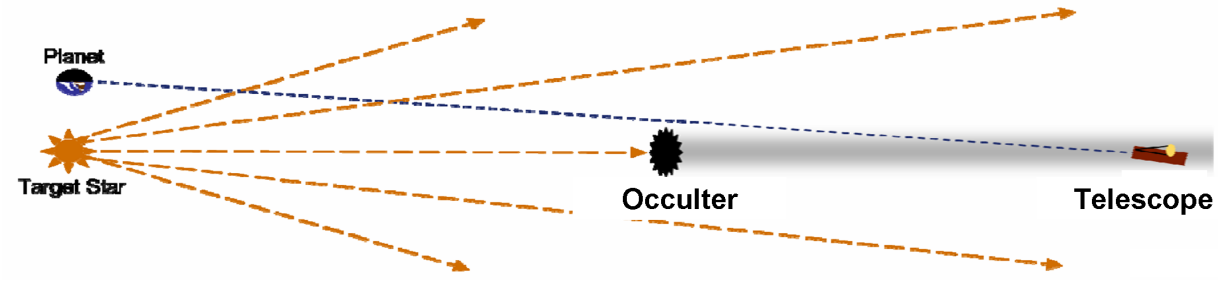

Figure 1. Occulter-based extra-solar planet-finding mission diagram[3]

In this paper, we study the optimal configuration of satellite formations consisting of a telescope and multiple occulters. The objective is to enable the imaging of the largest possible number of satellites with

*Mechanical and Aerospace Department, Princeton, NJ, 08544, USA.

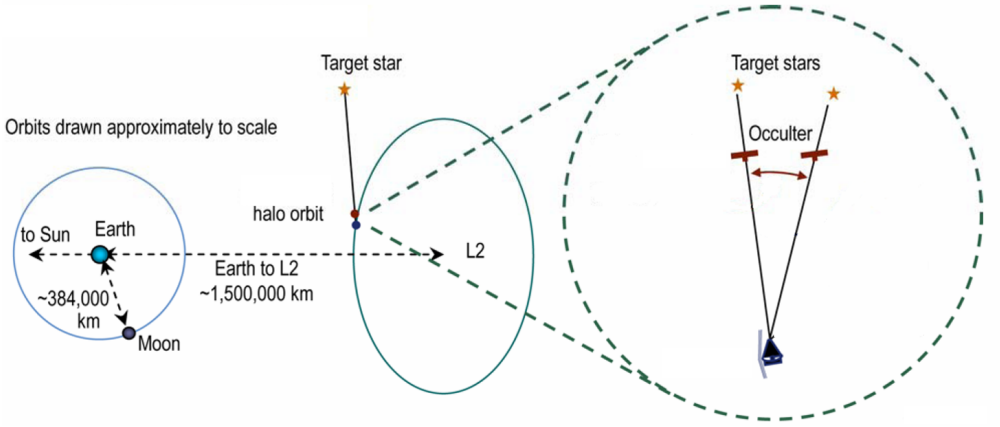

Figure 2. A schematic diagram of occulter mission orbits projected into the ecliptic plane[3]

.

minimum mass requirement which consists of the dry mass of the spacecrafts and the total fuel requirement for the formation. As the number of occulters increases, so does the dry mass; however, the total fuel requirement decreases. The scientific achievement, that is, the number of planetary systems that are imaged, is higher. This paper enables a trade-off study, using more satellites in terms of cost and scientific achievement.

The periodic and quasi-periodic orbits around the libration points were studied in detail by Kolemen & Kasdin.[4] In section II, we outline the procedure and the main results of this paper. First, we identify the fuel-free maximum sky coverage orbits. Quasi-Halos are good candidates for occulter placement, as they are fuel-free orbits and have large sky coverage with respect to the Halo orbit, where the telescope is placed. With the aim of identifying these orbits, we developed a new fully numerical method which employs multiple Poincaré sections to find quasi-periodic orbits. The main advantages of this method are the small overhead cost of programming and very fast execution times, robust behavior near chaotic regions that leads to full convergence for a given family of quasi-periodic orbits, and the minimal memory required to store these orbits. This method reduces the calculation of the search for the two-dimensional invariant torus to a search for the closed orbits, which are the intersection of the invariant torus with the Poincaré sections. Truncated Fourier series are employed to represent these closed orbits. The flow of the differential equation on the invariant torus is reduced to maps between the consecutive Poincaré maps. A Newton iteration scheme makes use of the invariancy of the circles of the maps on these Poincaré sections in order to find the Fourier coefficient that define the circles to any given accuracy. A continuation procedure that uses the incremental behavior of the Fourier coefficients between close quasi-periodic orbits is utilized to extend the results from a single orbit to a family of orbits. The Quasi-Halo and Lissajous families of the Sun-Earth Restricted Three-Body Problem (RTBP) around the L1 and L2 libration points are obtained via this method. Via a new collocation algorithm, these results are then extended to find the real quasi-periodic families of the full ephemeris solar system where the effect of all the planets at their real locations is taken into account.

Subsequently, we study the best configuration of the constellation. This is a highly complex dynamical, time-dependent optimization problem. To gain insight, we first solve the control problem of the two-satellite formation, consisting of the telescope and an occulter. The objective is to enable the imaging of the largest possible number of planetary systems with minimum fuel consumption. The control problem can be separated into two parts; first, the line-of-sight (LOS) control of the formation during imaging, and second, the trajectory control for realignment between imaging sessions. Realignment is far more dominant in fuel consumption then LOS control. We therefore focus on the realignment problem to get an estimate the total fuel consumption.

The optimal control of the realignment is studied in detail in another publication.[5] In section III, we outline the procedure and the main results of this paper. First, the optimal control problem of the realignment is solved. This gives us the minimum energy and minimum time trajectories that take the occulter from a given star LOS to another LOS. The solution to the optimal control problem is implemented using three different methodologies. First, a Lambert-like approach is employed, where the control consists of two large Delta-V maneuvers at the beginning and at the end of the trajectory. The second approach is to discretize

the optimal control problem and solve a high-dimensional nonlinear optimization problem via a sequential programming (SQP) method. The third approach uses the Euler-Lagrange formulation, i.e. the adjoint method, in order to find a continuous thrust solution. This method is very fast, thus enabling millions of trial cases to be solved. This reduces the Delta-V solution of the dynamical optimization problem to an approximate function of the major parameters of the problem such as the time-to-go, the angular separation, and the distance between the telescope and the occulter. All three methods are applied, and the results of each method are compared with one another.

After finding the relevant minimum-fuel trajectories between all the target stars, the sequencing and timing of the imaging session is examined in order to minimize global fuel consumption. By including the constraints imposed by the telescopy requirements, the problem becomes a Dynamic Time-Dependent Traveling Salesman Problem with dynamical constraints. Branch-And-Cut and Tabu Search heuristic methods are employed to solve the Traveling Salesman Problem (TSP).

Having solved the single occulter problem, we study the best configuration of the constellation of multiple occulters. This problem consists of the initialization of the constellation, and the selection of each occulter's imaging itinerary.

To reduce the problem to a solvable one, we simplify it by assuming that each of the parts can be studied independently. Then, the initialization problem becomes an optimization of the size and phases of all the occulters such that, in the absence of any control, the occulters' trajectories come close to intersecting the maximum number of star LOS within a given time span. This provides us with approximate information about the timing and sequencing of the imaging sessions of each occulter.

The global optimization problem of finding each occulters' itinerary is transformed into a TSP as was the case for the single occulter. Then, TSP is solved with the initial feed, which is obtained from the previous initialization problem. The same technique as that of the single occulter TSP is employed. The last two procedures of initialization and TSP-solving are repeated until a reasonable global solution is achieved. These results gives us an approximate Delta-V budget for different configurations, which will be useful for a trade-off study of various constellations.

II. Dynamics around L2

A. Families of Periodic and Quasi-Periodic Orbits Around L2

1. Periodic Orbits

The linear six-dimensional phase space around L2 is a *center* $\times$ *center* $\times$ *saddle*. For energy values close to that at L2, where it is sufficient to consider only the linear approximation to the equations of motion, there exist two families of periodic orbits; the Horizonal Lyapunov orbits, which are in the ecliptic plane, and the horizontally symmetric figure-eight-shaped Vertical Lyapunov orbits. As the energy is increased, and nonlinear terms become important, the linear phase space is broken and a new periodic family, Halo orbits, bifurcate from the Horizontal Lyapunov orbit family. These orbits are three-dimensional and asymmetric about the ecliptic plane. Figure 3 and figure 4 show the three distinct periodic orbit families around L2.

2. Quasi-Periodic Orbits

The four-dimensional center manifold around L2 is occupied by quasi-periodic orbits of two different families: The Lissajous family around the Vertical Lyapunov orbits, and the Quasi-Halos around the Halo orbits. These quasi-periodic orbits reside on invariant tori about the corresponding periodic orbit. To visualize this four-dimensional center manifold, which consists of all the periodic and quasi-periodic orbits, on a two-dimensional figure, we need to constrain the center manifold by two dimensions. A convenient way of achieving this is to choose periodic and quasi-periodic orbits which have the same energy, and to take a Poincaré section when these orbits cross the ecliptic plane. When we do this we obtain figure 6. Since this is a Poincaré section, the equilibrium points correspond to the periodic orbits of the original system, while the closed curves correspond to the quasi-periodic orbits. This correspondence is shown in figure 6. Detailed approaches for obtaining these orbits are discussed in the following sections.

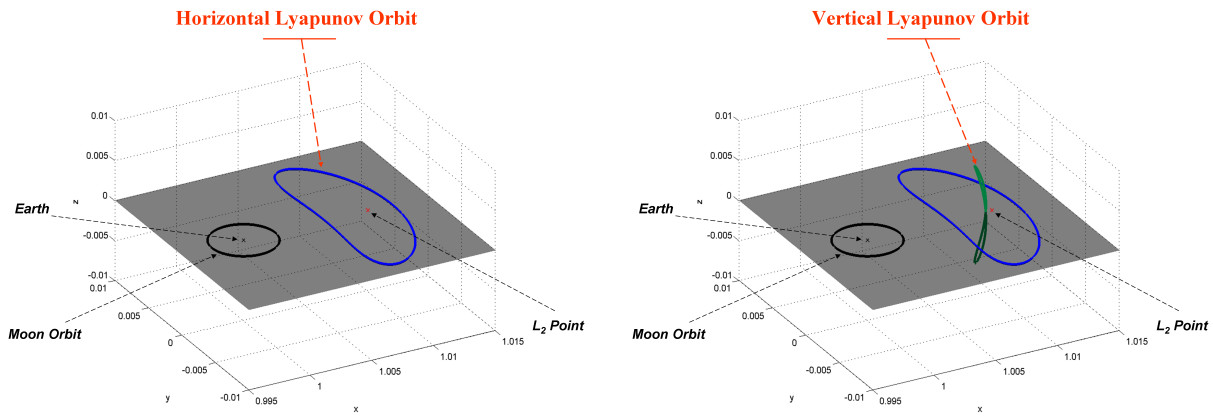

Figure 3. Horizontal and Vertical Lyapunov periodic orbits around L2 libration point.

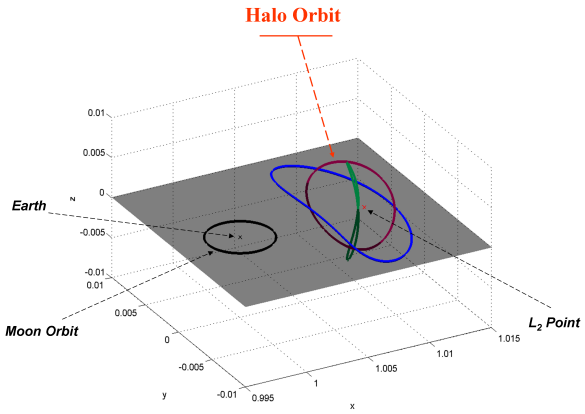

Figure 4. Halo periodic orbit around L2 libration point.

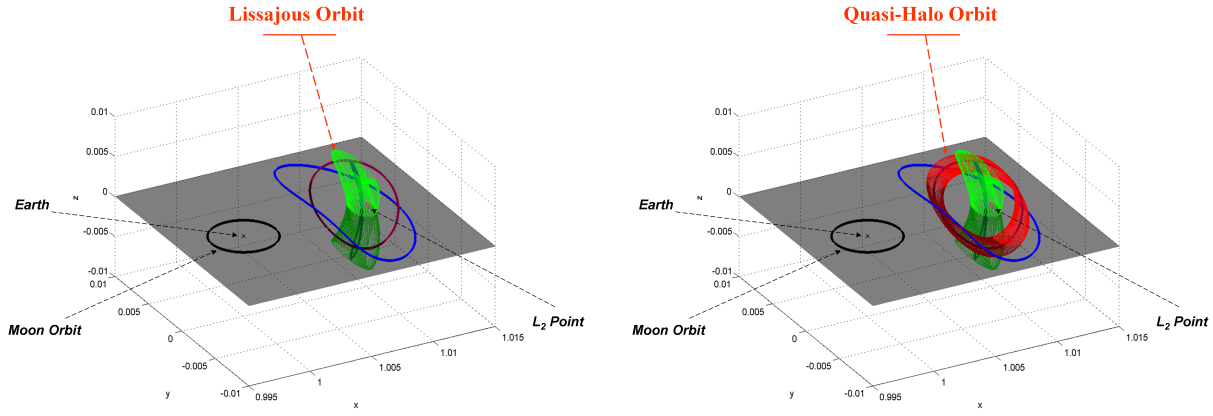

Figure 5. Quasi-periodic orbits around L2 libration point

B. Finding Quasi-Periodic Orbits via Multiple Poincaré Sections

We identify three main challenges associated with finding quasi-periodic orbits. The first is to minimize the time it takes to program the software that numerically solves for the orbits. This reduces the threshold for

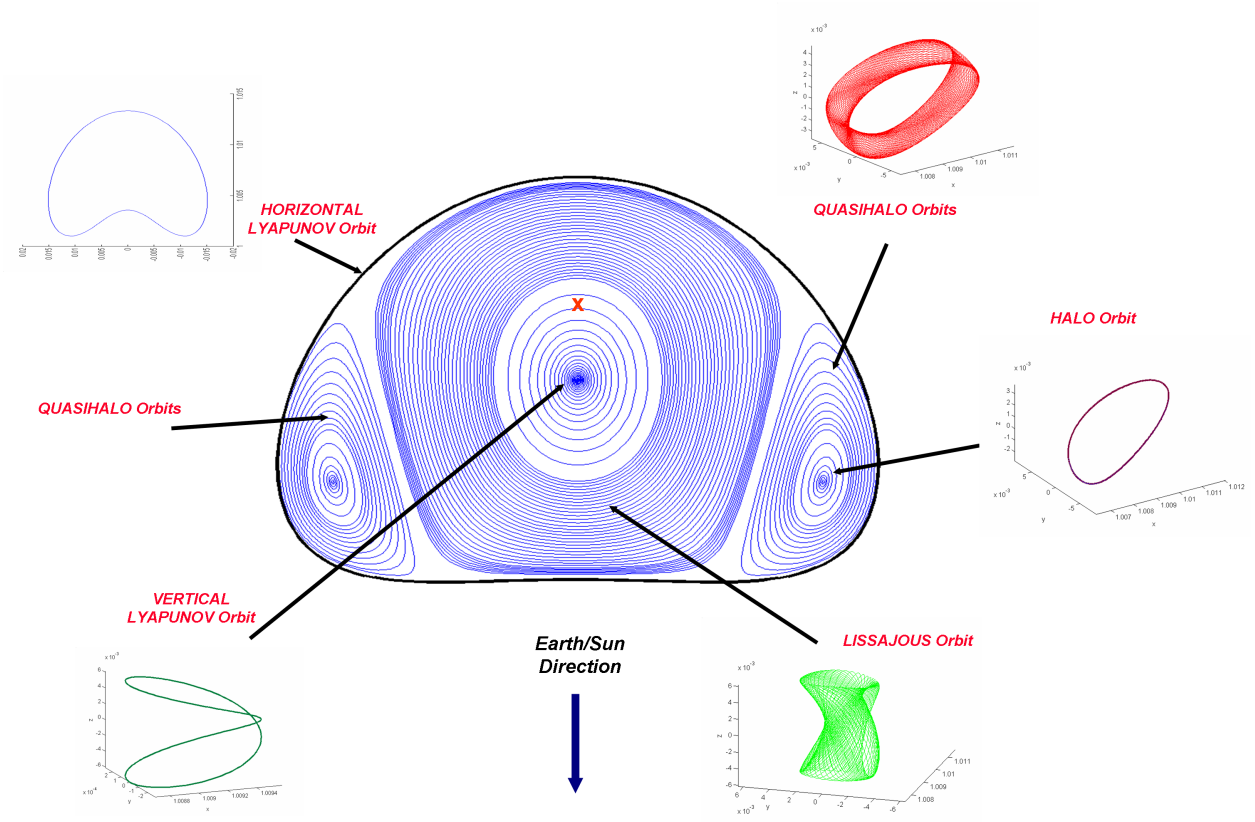

Figure 6. All the periodic and quasi-periodic orbits around L2 shown on a Poincaré section of the ecliptic plane

researchers who work on trajectory design. The second is to achieve reasonable execution times, allowing results to be obtained quickly and "on the go". The third is to improve the robustness of the method in order to get the very large regions of attraction that are needed to obtain the full families of quasi-periodic orbits.

Symbolic methods such as the Lindstedt-Poincaré method[6] and the reduction to the center manifold,[7,8] which depend on series expansions, are very slow because an exponential increase in the number of coefficients is needed for every additional increase in the order of expansion. The speed problem can be overcome to a great extent by programming a symbolic manipulator for the problem of interest, but this leads to a significant increase in programming time. More importantly, some of these techniques have instability problems near resonances.

This led us to consider fully numeric methods. However, instead of taking a mesh on the whole surface, which requires many points and is thus memory and CPU intensive, we considered only a section on the torus containing the quasi-periodic trajectories and thus represented the full torus by only points on this section. These points must be integrated for one period at each iteration step. The initial errors in our estimation of the section increase exponentially with the highest Lyapunov exponent as the integration time increases. This is of great concern, especially for the RTBP L2 case where the Lyapunov exponent is more than 10^3. The effect is more dramatic near resonance and chaotic regions. To overcome this problem, we reduce the integration times by taking multiple sections on the torus, integrating only between the consecutive Poincaré sections. The methodology is parallel to the multiple shooting method used in two-point boundary value problems.[9]

In what follows, we first introduce the methodology by explaining the procedure for a single Poincaré

section. The results are then extended to multiple Poincaré sections. We discuss different implementations using Poincaré sections on phase space and time. Finally, a continuation method to find the full family of quasi-periodic orbits is introduced.

1. *Finding Invariant Tori via a Single Poincaré Section*

The first step in the procedure is to find a convenient Poincaré section. This can be either a section in time or space. For visualization purposes, we assume that the section is taken in phase space, as shown in figure 7. When choosing the plane of the section, the main concern is to ensure that the velocity vector of the quasi-periodic orbit is as transverse to the plane of section as possible. This reduces the possibility that the integrated points will not return to the Poincaré section. Thus, a good candidate for the Poincaré section is the plane perpendicular to the velocity of the halo orbit section. However, for the RTBP, a simple section on the ecliptic plane is also suitable. We used both types of Poincaré sections for the results in this paper.

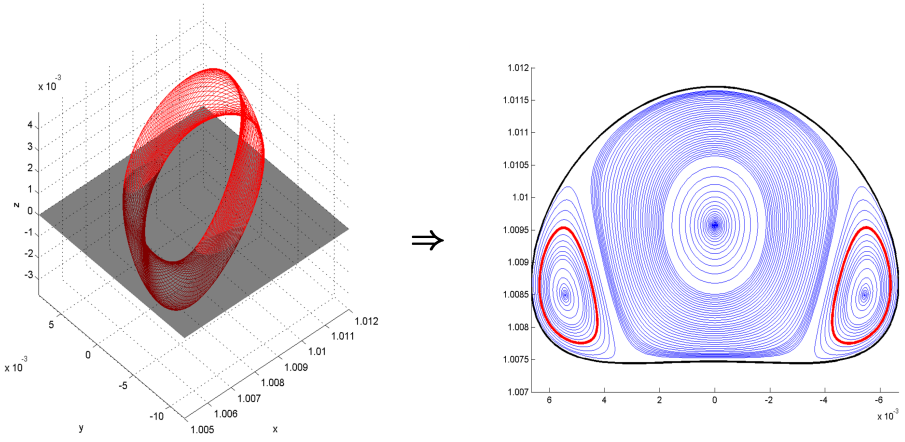

Figure 7. Converting the search for a torus problem of a differential equation to the search of the circle of a map

Instead of trying to find the torus of the full ordinary differential equation, our next aim is to find the closed orbits of the Poincaré map. We expand the closed orbit in a truncated Fourier series with the expansion parameter θ, the angle on the closed orbit. For instance, in the case where we took the Poincaré section on the ecliptic plane, i.e. $z = 0$, the expansion parameter becomes $\theta = atan(\frac{y-y_{halo}}{x-x_{halo}})$. It is important to note that we need to parameterize the system such that every point on the closed orbit is uniquely defined by one value of the parameter. For closed orbits with complex shapes, other parameters, such as the ratio of the arc length between a specific point on the orbit and the full arc length of the closed orbit,[10] should be used to ensure uniqueness. For the RTBP, however, this simple parameter gives satisfactory results.

We then take sample points, $\mathbf{X_0}$, on the closed orbit:

$$\mathbf{X_0} \quad = \quad \sum_{n=-n_m}^{n_m} Q_n e^{in\theta}. \tag{1}$$

We map these points, $\mathbf{P}(\mathbf{X_0})$, by integrating the equations of motion until they intersect the Poincaré section,

$$\mathbf{X_T} \quad = \quad \mathbf{P}(\mathbf{X_0}) \quad = \quad \phi_{T(\mathbf{X_0})}(\mathbf{X_0}); \tag{2}$$

The first variations of these equations are integrated along with $\mathbf{X_0}$, for later use in the iteration process. As seen in figure 8, finding the quasi-periodic orbit is then reduced to solving for the Fourier coefficient vector $\mathbf{Q}$ that satisfies the following equation,

$$F(\mathbf{Q}) \quad = \quad \mathbf{X_T} - \sum_n Q_n e^{in\theta(\mathbf{X_T})} \quad = \quad 0 \tag{3}$$

One advantage of this formulation is that we can use a Newton iteration and get quadratically convergent solutions. In Newton's iteration, an initial guess $\mathbf{Q^1}$ is iterated according to

$$DF(\mathbf{Q^j}) \cdot (\mathbf{Q^{j+1}} - \mathbf{Q^j}) \quad = \quad -F(\mathbf{Q^j}) \tag{4}$$

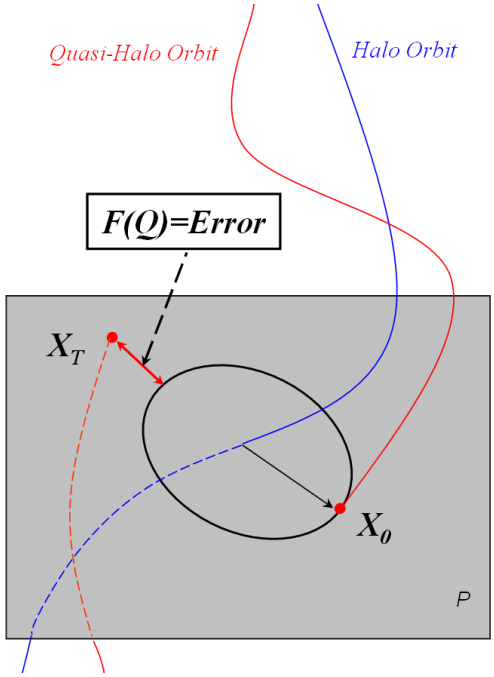

Figure 8. Schematic illustration of the numerical procedure for finding the invariant torus

until a satisfactory answer is reached. To find an explicit form for this equation, we write $\mathbf{X}$ as a matrix multiplication,

$$\mathbf{X} \quad = \quad \sum_n Q_n e^{in\theta} \quad = \quad M(\theta) \cdot \mathbf{Q} \tag{5}$$

F then becomes,

$$\begin{aligned} F(\mathbf{Q}) &= \mathbf{X_T} - \mathbf{X}_{\theta_{\phi(\mathbf{X_0})}} \\ &= \phi(M \cdot \mathbf{Q}) - M_{\theta_{\phi(M\ \mathbf{Q})}} \cdot \mathbf{Q} \end{aligned} \tag{6}$$

We then take the derivative with respect to $\mathbf{Q}$,

$$\begin{aligned} DF(\mathbf{Q}) &= \frac{dX_T}{dX_0}\frac{dX_0}{dQ} - \frac{dX}{d\theta}\frac{d\theta}{dX_T}\frac{dX_T}{dX_0}\frac{dX_0}{dQ} \\ &= DP \cdot M - (DM_{\theta_{\phi(M\cdot\mathbf{Q})}} \cdot \mathbf{Q}) \cdot \frac{d\theta}{dX_T} \cdot DP \cdot M \end{aligned} \tag{7}$$

where DP is the differential of the Poincaré map obtained from the first variation of the map integrated with $\mathbf{X}$. Employing Newton's iteration, solutions converge usually within 3-4 iterations. An example of an iteration procedure is shown in figure 9. Here the sample points are shown with crosses and the return maps are shown by circles. After four iterations, all the estimates and the return maps are aligned on the same closed orbit.

2. Extension to Multiple Poincaré Sections

In order to overcome the potential instability that results from the long integration times, the invariant torus can be cut by several Poincaré sections, as mentioned before. Figure 10 shows the closed orbits which we obtain when the tori of interest are cut with multiple sections. As a result, all of these closed orbits in figure 10 will be searched instead of only the single one in the previous sub-section.

The numerical procedure is similar to the single Poincaré section method but in this case, $\mathbf{Q}$, the vector containing the Fourier coefficients, is composed of the Fourier coefficients of each of the closed orbits,

$$q_i \quad = \quad \mathbf{Q}^t_{n_i}, \quad i = 1, 2, \ \ldots \ , N_{Poincaré\ sections} \quad n = 1, 2, \ \ldots \ , N_{Fourier\ series} \tag{8}$$

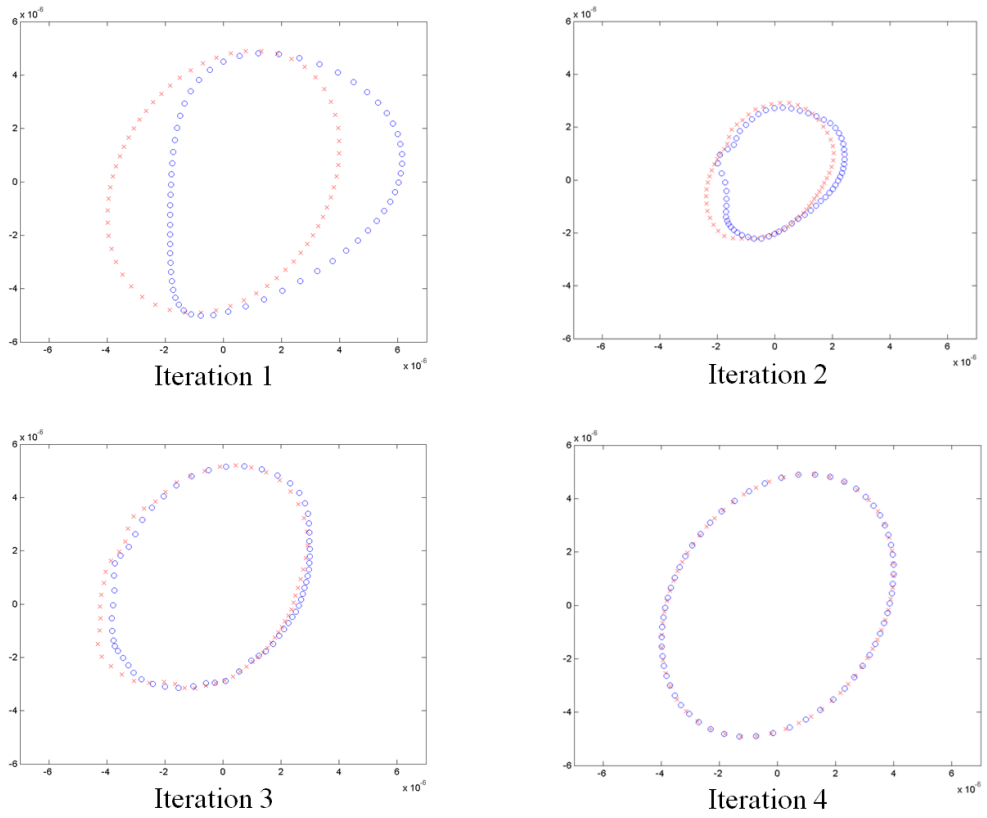

Figure 9. Iteration procedure in steps

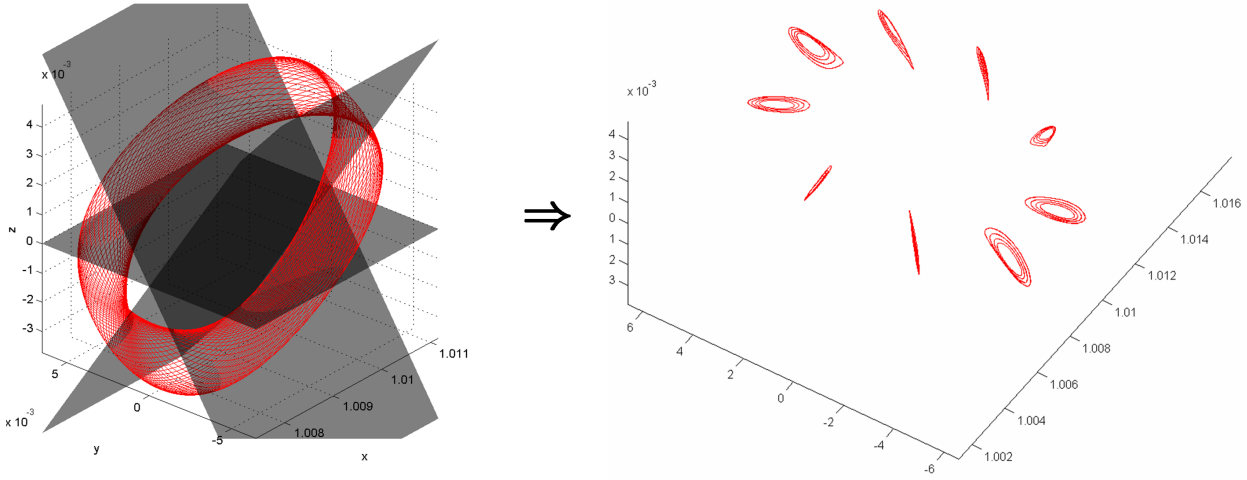

Figure 10. Multiple Poincaré Section Procedure: Closed orbits obtained by sectioning invariant tori

The invariance condition for these closed orbits to be on the same torus is

$$F(\mathbf{Q}) \;=\; F\begin{pmatrix} q_1^t \\ q_2^t \\ \vdots \\ q_{N-1}^t \\ q_N^t \end{pmatrix} \;=\; \begin{pmatrix} \phi(M\cdot q_1) \\ \phi(M\cdot q_2) \\ \vdots \\ \phi(M\cdot q_{N-1}) \\ \phi(M\cdot q_N) \end{pmatrix} - \begin{pmatrix} M_{\theta_{\phi(M\cdot q_1)}}\cdot q_2 \\ M_{\theta_{\phi(M\cdot q_2)}}\cdot q_3 \\ \vdots \\ M_{\theta_{\phi(M\cdot q_{N-1})}}\cdot q_N \\ M_{\theta_{\phi(M\cdot q_N)}}\cdot q_1 \end{pmatrix} \;=\; 0. \tag{9}$$

Finally, as before, we apply Newton's iteration to root finding,

$$DF(\mathbf{Q}^j)\cdot(\mathbf{Q}^{j+1}-\mathbf{Q}^j) \;=\; -F(\mathbf{Q}^j). \tag{10}$$

3. *Different Implementations*

Depending on how we choose the Poincaré section, the procedure can be implemented in different ways. If we take a Poincaré section in phase space, the four-dimensional center manifold is constrained by two dimensions. The first dimensional constraint is due to the Poincaré section, and the second one is due to the fact that the closed orbit we are interested in is one-dimensional. As a result, we are left with two degrees of freedom to specify a unique orbit. Thus, we can specify two constraints, which are properties of the orbit that are of interest. We can, for example, specify the Hamiltonian and the size of the orbit. Since we are working on a Poincaré section, size can be specified by the area which is enclosed by the closed orbit. Then, the constraint vector is augmented to include the new constraints,

$$F \;=\; [F\,;\; H_{fixed} \,-\, H(\mathbf{Q})\,;\; Area_{fixed} \,-\, Area(\mathbf{Q})]. \tag{11}$$

Another implementation is to take a Poincaré section in time. This way we can specify the period of the quasi-periodic orbit along with the integration direction for the return map. This is especially important for space missions that require all the spacecraft to stay close to one another at all times. In this case, we have one more degree of freedom to specify a unique orbit. We can do this by augmenting the error vector with a new constraint, such as the projected size along one direction,

$$F \;=\; [F\,;\; Size_{fixed} \,-\, Size(\mathbf{Q})\,;\; \ldots\,]. \tag{12}$$

4. *Continuation Procedure*

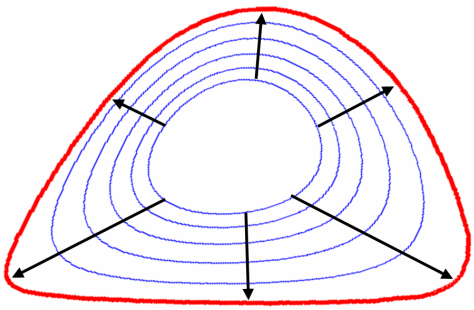

Figure 11. Continuation in the area variable

Once we obtain the Fourier coefficients for a given orbit, we would like to extend these results to find the complete family of quasi-periodic orbits. In figure 11, the continuation in the area variable is shown. While there is no intuitive way to continue the coordinate variables, $[x, y, z, \dot{x}, \dot{y}, \dot{z}]$, the continuation of the Fourier coefficients is straight-forward, since they vary incrementally between sufficiently close quasi-periodic family members. A low-order polynomial fit is thus sufficient for continuing these parameters. Even a very simple linear continuation in the area variable, A, gives satisfactory results,

$$\mathbf{Q}_{k+1} \;=\; \mathbf{Q}_k + (A_{k+1}-A_k)\frac{\mathbf{Q}_k-\mathbf{Q}_{k-1}}{A_k-A_{k-1}}. \tag{13}$$

C. Comparison of the Results

The Poincaré section in time, where we specified the orbit period, is shown in figure 12. Here we compare the results to Gómez et al.'s.[6] By specifying the period of all the orbits to be the same as the base halo orbit's, we can ensure that the spacecraft stay close at all times. This is of great importance particularly for natural, control-free, formation-flying missions. The main advantage of the Poincaré section approach is that, due to the numerical nature of the algorithm, the calculations take only a few minutes of computation time, with minimal programming requirement. Note that, since the Hamiltonians for these orbits are not equal to one another, the orbits may intersect.

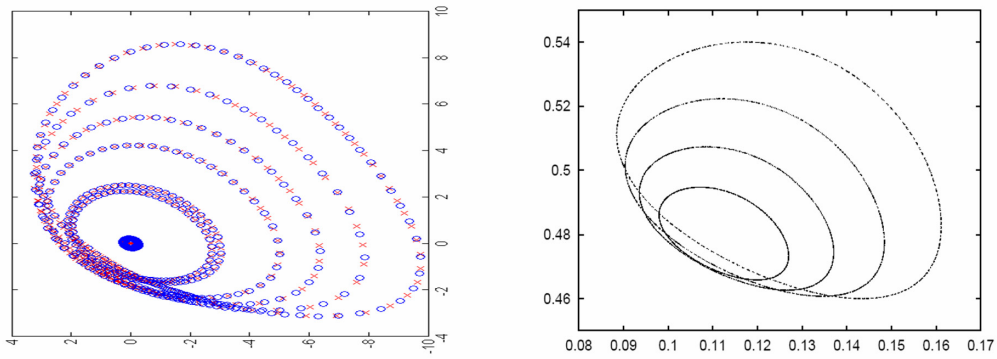

Figure 12. The Poincaré section of the invariant tori, where the period of all the orbits is equal to that of the base halo orbit. The multiple Poincaré section method is employed on the left while the Lindstedt-Poincaré method is used on the right.[6]

Utilizing the multiple sections approach, we found the complete Quasi-Periodic Orbit Families around the libration points. Figure 13 shows the Poincaré section of the quasi-periodic family with constant energy on the ecliptic plane, compares the results obtained by our multiple Poincaré method with Gómez & Mondelo's refined Fourier analysis[11,12] and Gómez et al.'s Lindstedt-Poincaré analysis.[6] While Lindstedt-Poincaré analysis[6] can not obtain the complete families and a cluster of parallel computers was required to get the complete families with the refined Fourier analysis,[11,12] our method obtains the complete set of quasi-periodic orbits and the computation of the full families takes only a few minutes on a 2.15 GHz Intel Pentium processor.

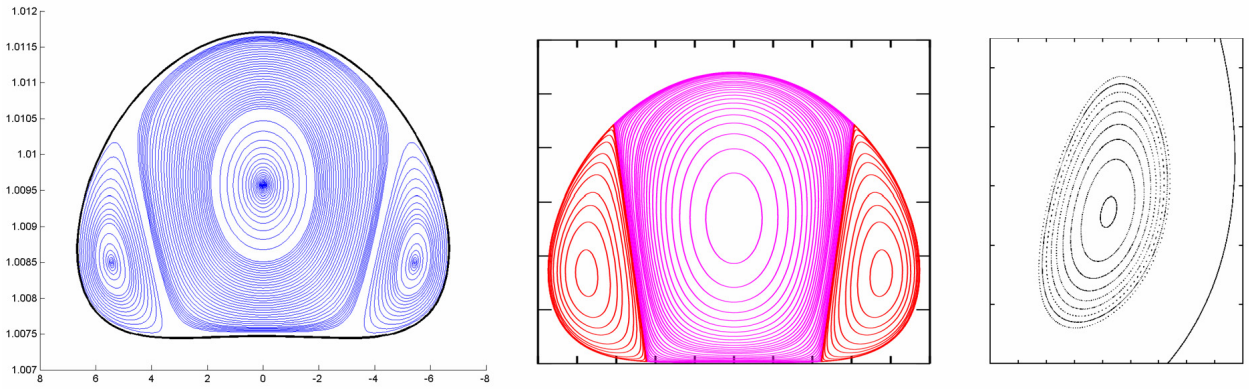

Figure 13. The Poincaré section of the complete quasi-periodic family around L2 with energy that is equivalent to the 500,000 km-sized halo orbit on the ecliptic plane (on the left). Similar results from Gómez & Mondelo[11,12] (in the middle) and Gómez et al.[6] (on the right).

D. Transfer of the Quasi-Periodic Orbits to the Full Ephemeris Model

The quasi-periodic orbits obtained above reside on two-dimensional surfaces around the libration points of the RTBP. These orbits do not exist in the real Solar system due to the eccentricity of the Earth's orbit and

the perturbing effects of many celestial bodies. Nevertheless, the full ephemeris model, JPL DE-406, gives us orbits that have almost identical properties to the orbits found in the simplified problem.

Halo and Quasi-Halo orbits around the libration points are very unstable. Thus, we employ a collocation algorithm, which is a very robust boundary value problem-solving technique. The aim of the algorithm is find the orbits in the full ephemeris model that stay close to the RTBP solutions found previously. The algorithm takes as its initial guess the RTBP orbits, and "transfers" these quasi-periodic orbits of RTBP to the full ephemeris model.

Generally, collocation algorithms are used to solve boundary value problems (BVP) of first-order differential equations

$$\dot{x} = f(x), \qquad a \leq t \leq b \tag{14}$$

which are subjected to boundary conditions

$$g(x(a), x(b)) = 0. \tag{15}$$

However, in our case we do not know the exact position of the initial and final states. Thus, we solve for the state vector, x , subjected only to the differential equation constraint. We proceed by discretizing the time and state variables at N points along the trajectory

$$a = t_0 < t_1 \ldots < t_{N-1} < t_N = b. \tag{16}$$

We approximate the state by a piecewise cubic polynomial function $x_i = S(t_i)$. If our guess is sufficiently close to the real solution, the discretized quadrature equation, which corresponds to the differential equation, gives the following constraint at every point

$$0 = \Phi(t_i, x_i) = -x_{i+1} + x_i + \frac{h_i}{6}\left(f(x_i) + f(x_{i+1})\right) + \frac{2h_i}{3}\left(f(\frac{x_i + x_{i+1}}{2}) - \frac{h_i}{8}\left(f(x_{i+1}) - f(x_i)\right)\right) \tag{17}$$

where

$$h_i = t_{i+1} - t_i. \tag{18}$$

Without adding any boundary conditions, we solve the N dimensional nonlinear equation given by $\Phi(t_i, x_i) = 0$, using Newton's method, following Kierzenka et al.'s[13] *bvp4c* implementation.

Figure 14 shows the result for a 150,000 km radius Quasi-Halo around the Sun-Earth L2 point, with a base Halo orbit of 500,000 km out-of-plane amplitude.

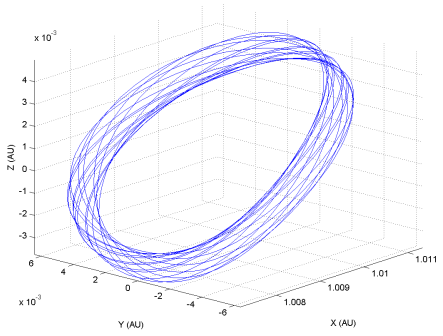

Figure 14. Three-dimensional view of a Quasi-Halo orbit with 150,000 km separation from the base Halo orbit in the JPL DE-406 model

The collocation algorithm performed robustly around the Sun-Earth L2 point where the missions of our interest will be located. We also implemented the multiple shooting algorithm, developed by Gómez et al.[6] for the Quasi-Halo refinement. The obtained results and the computation time from both methods are similar. Further comparisons, including the more computationally challenging orbits of the Earth-Moon system, will be performed as part of future research.

III. Optimization of the Mission

Figure 15 shows an example of the relative motion of an occulter placed on a Quasi-Halo orbit, with respect to the telescope on a Halo orbit. As seen in the figure, the occulter covers the full sky, which makes possible the imaging all the target stars. This is done without any fuel consumption, and while keeping the distance approximately fixed, since the Quasi-Halo orbits are part of the dynamical structure around the L2 libration point, which enables the spacecraft to ride the wave. However, a major drawback of placing a spacecraft on a Quasi-Halo orbit is that the periods of these orbits around the Halo are roughly 6 months. As a result, single spacecraft located on a Quasi-Halo orbit will not be able to fulfill the requirement of imaging a target approximately every 1 to 2 weeks.

There are two possible approaches to this problem. The first approach employs a single occulter with fuel-intensive trajectory control, while the second one employs multiple occulters that use the natural dynamics more efficiently, thus minimizing fuel consumption per spacecraft. While employing multiple spacecraft increases the mission's total mass, because of the duplication of all the components, it reduces the maximum thrust, which enables us to use smaller thrusters, and which reduces the mass per spacecraft. In addition, redundancy in the multiple spacecraft system will be an insurance in case of a malfunctioning of one of the occulter systems.

This section aims to arrive at the algorithms to optimize the different mission scenarios from beginning to end, and to reduce the complexities of the various missions to simple graphs, where the side-by-side comparison of the advantages and disadvantages of these missions is possible. This makes possible a trade-off study, using more satellites, in terms of cost, i.e. the total Delta-V for the mission, and scientific achievement, i.e. the number of planetary systems that are imaged.

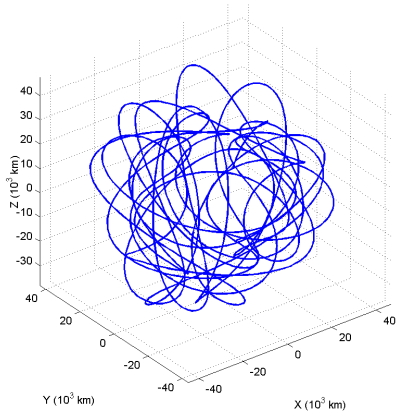

Figure 15. Relative position of the occulter with respect to the telescope in the inertial frame (Mean Radius 30,000 km)

For ease of comparison, all the missions scenarios discussed from here on assume a base Halo orbit around L2 with an out-of-plane amplitude of 500,000 km.

A. Optimization of the Single Occulter Mission

In this section, we study the control of the two-satellite formation consisting of a telescope and an occulter. The objective is to enable the imaging of the largest possible number of satellites with minimum fuel consumption. The control problem can be separated into two parts; first, the line-of-sight (LOS) control of the formation during imaging, and the trajectory control for realignment between imaging sessions. Here we focus on the latter, since the realignment dominates the Delta-V budget.

1. Finding the Delta-V's between star positions

First, we look at the optimal control problem of finding the trajectory that takes the occulter from the first star LOS to the second LOS. If we fix the separation of the occulter and the telescope, the problem

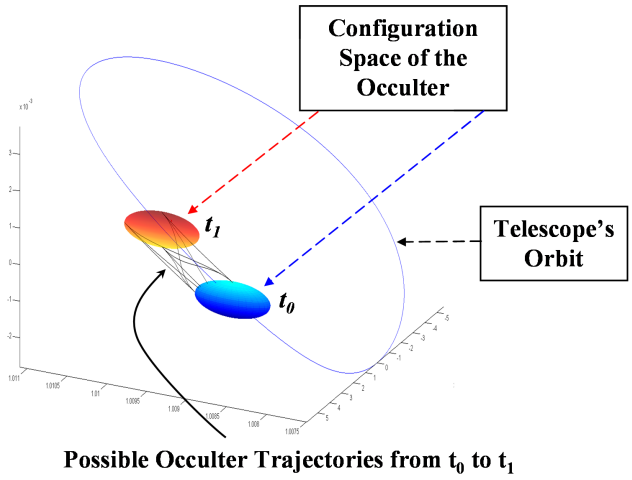

Figure 16. The sphere of possible occulter locations about the telescope at two times, and example optimal trajectories connecting them.

becomes one of finding an optimal trajectory between two, two-dimensional surfaces as shown in figure 16. This optimization is done using three different methodologies in Kolemen & Kasdin.[5] First, a Lambert-like approach is employed, where the control consists of two large Delta-V maneuvers at the beginning and at the end of the trajectory. This forms a forms such that

The second approach is to discretize the optimal control problem and solve a high-dimensional nonlinear optimization problem via a SQP algorithm. For this purpose, LOQO[14] and IPOPT[15] interior method SQP-solver software was utilized. The third approach uses the Euler-Lagrange formulation, i.e. the adjoint method, in order to find a continuous thrust solution. This method is very fast, thus enabling millions of trial cases to be solved. This reduces the Delta-V solution of the dynamical optimization problem to an approximate function of the major parameters of the problem such as the time-to-go, the angular separation, and the distance between the telescope and the occulter. All three methods are applied and the results of each method are compared with one another in Kolemen & Kasdin.[5] In figure 17, the optimal Delta-V results from these millions of optimizations are averaged, giving Delta-V as an approximate function of Radius and LOS angle for a transfer time of 2 weeks.

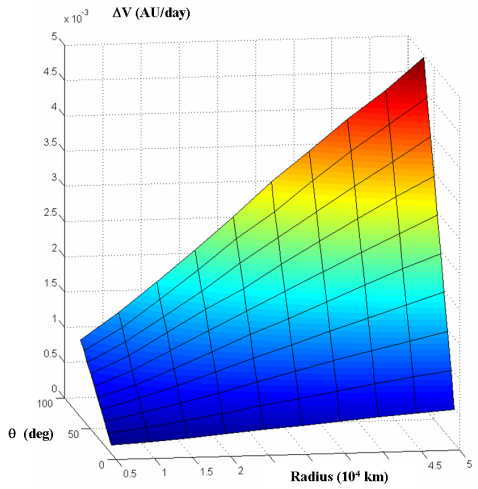

Figure 17. Surface of optimal Delta-V's as a function of distance from the telescope and angle between the LOS vectors of consecutively imaged stars (Δ t = 2 weeks)

In order to have a more realistic mission analysis, we used the top 100 TPF-C target stars, and found the Delta-V for realignment between each target, as shown in figure 18.[16]

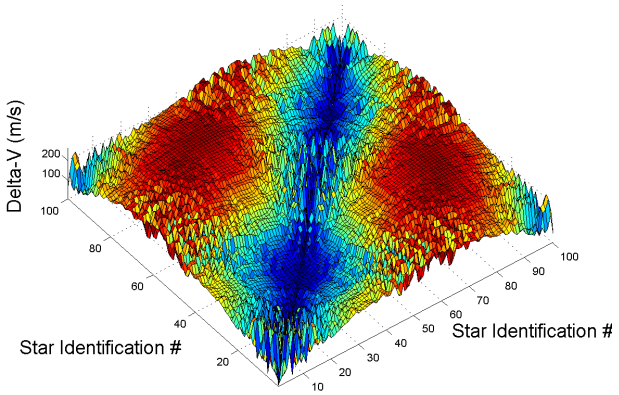

Figure 18. Minimum Delta-V needed to realign the occulter between the Top 100 TPF-C targets. The X and Y coordinates denote the identification number of the stars, and the Z coordinate denotes the minimum Delta-V to realign from X(i) to Y(j) in m/s.

2. Dynamic Time-Dependent Traveling Salesman Problem

After finding the relevant minimum-fuel trajectories between any given star-imaging sessions, the sequencing and timing of the imaging session is examined, in order to minimize global fuel consumption. The reflection of sunlight from the occulter to the telescope interferes with the imaging of the planetary system. This constraints the occulter to be approximately between 45 to 95 degrees from the Sun direction (See figure 19).

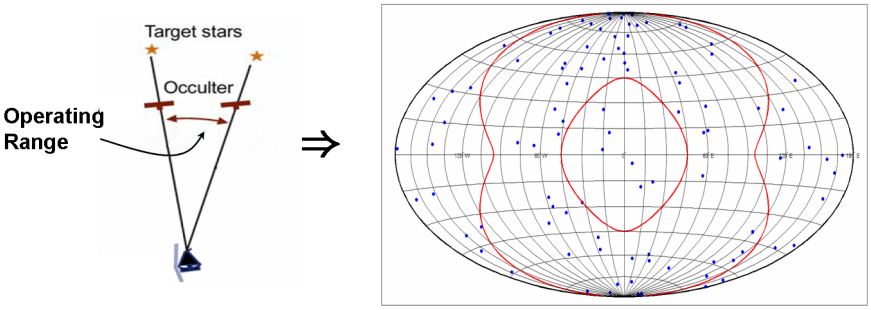

Figure 19. Operating range restriction of the occulter shown on a skymap

By including the constraints imposed by the telescopy requirements, the problem becomes a Moving Target Time-Dependent Traveling Salesman Problem with dynamical constraints (See figure 20). The problem reduces to finding the minimum sum sequence that connects the rows and columns of the time-dependent TSP matrix. There are other constraints that we impose on the sequencing that are not shown on this figure. To ensure that the images of the planetary system of interest do not produce the same results, the minimum time between re-imaging of a target is 6 months. We randomly choose which stars are to be revisited, and how many times. While we do have the capability to ensure that there are no planets along the LOS, and to take into account the albedo effect of the Moon, we choose not to consider these minor constraints at this stage of optimization in order to save on computation.

In order to solve the global optimization problems, two heuristic, Tabu Search and Branch-And-Cut, methods were used. For problems of the size of our interest, the Tabu Search method[17] can find the best sequence for the no-constraint case very fast and very close to the optimal solution. However, it is not apparent how this method can be expanded to the case with dynamic constraints. The Branch-And-Cut algorithm, by contrast, can include constraints, but has a long computational time, and results may be far from optimal. We adopted a combined approach, using both methods, to enhance the solution of the TSP problem at hand. We started by solving the TSP problem via Tabu Search, each time assuming that

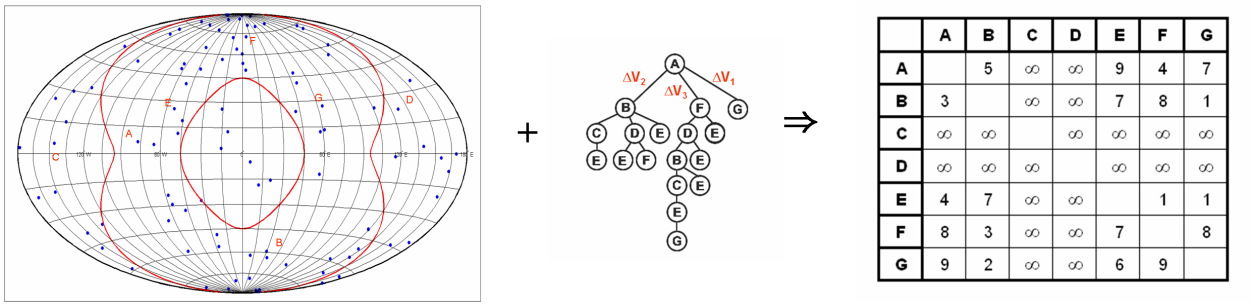

	A	B	C	D	E	F	G
A		5	∞	∞	9	4	7
B	3		∞	∞	7	8	1
C	∞	∞		∞	∞	∞	∞
D	∞	∞	∞		∞	∞	∞
E	4	7	∞	∞		1	1
F	8	3	∞	∞	7		8
G	9	2	∞	∞	6	9	

Figure 20. Including the constraints, the global optimization problem is converted to finding the best ordering of target stars, where the Delta-Vs between the targets are shown on the time-dependent TSP matrix. In the figure, unaccessible zones are shown as ∞.

constraints are fixed for all time, meaning that a target in a restricted zone is assumed to be permanently unobservable, even if that target will be visitable in several months' time. Patching the solutions we obtain from the Tabu Search, we formulate an initial guess for the optimal sequence, which we then feed to the Branch-And-Cut algorithm. A sample solution to the TSP using this methodology is shown in figure 21.

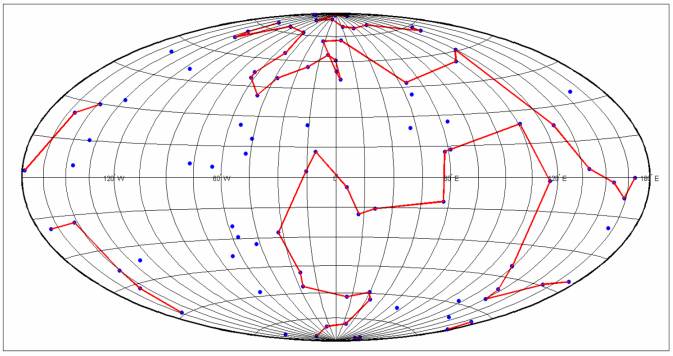

Figure 21. Global optimal solution to the single occulter TSP for 75 imaging sessions of the Top 100 TPF-C stars, with 2 weeks flight time between targets and no revisiting

The algorithms developed so far enable us to find the total minimal Delta-V requirement for a given mission. Figure 22 shows the averaged Delta-V obtained for the TPF-C top 100 stars, where we randomly picked which stars were to be revisited more than once as a function of the size of the formation and the average realignment time.

B. Optimization of the Multiple Occulter Mission

Having solved the single occulter problem, we study the best configuration of the constellation consisting of multiple occulters. This problem consists of the initialization of the constellation and the selection of each occulter's imaging itinerary.

To reduce to problem to a solvable one, we simplify it by assuming that each of the parts can be studied independently. First, we look at the initialization problem of the formation, where we use the dynamical insight from L2 and especially the properties of the Quasi-Halos. The optimization algorithms which were produced for the single occulter optimization are then employed for the itinerary of each star.

1. Initialization of the Formation

The initialization problem is an optimization of the $3 \times N$ parameters that uniquely define N Quasi-Halo orbits, namely size and the two-phase angles (R, θ_1, θ_2) of all the occulters, such that, in the absence of any control, the occulters' trajectories come close to intersecting the maximum number of star LOS within a

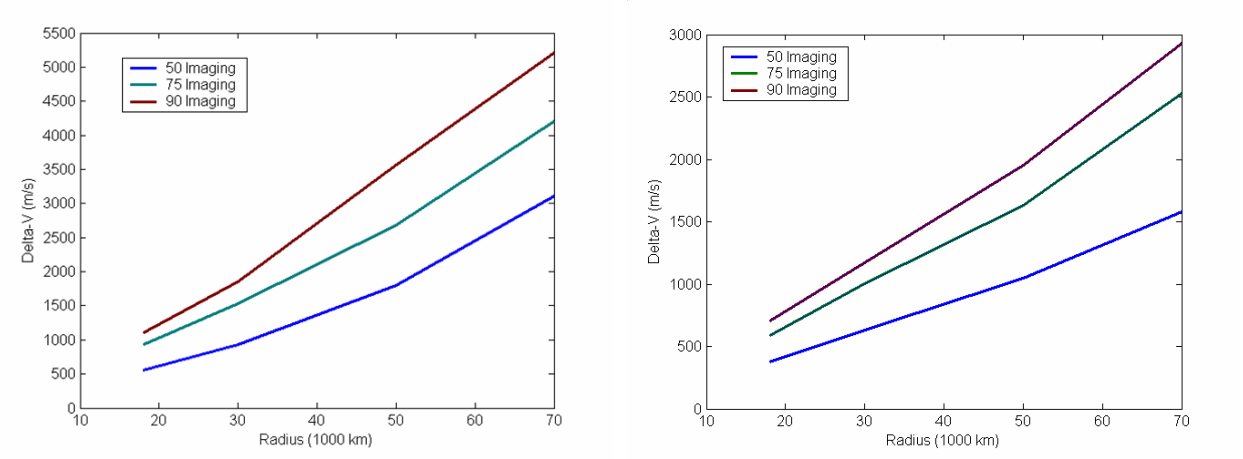

Figure 22. Minimum total Delta-V curves for the single occulter mission (Left: $\Delta t = 1$ week, Right: $\Delta t = 2$ weeks).

given time span. This is achieved by first choosing points in the (R, θ_1, θ_2) space that define the Quasi-Halos found in section II , and then integrating these forward in time (See figure 23). We transform the relative motion of these orbits with respect to the base Halo orbit to inertial coordinates; we then define an easily reachable region such as +5, -5 degrees from the path; and we find the number of targets that would be enclosed in this region. The $3 \times N$ parameters that give the highest number of targets in the union are taken to be the best initial guess for the formation.

This procedure provides us information on how to initialize the occulter formation, such that we make the most use of the natural dynamics for each occulter.

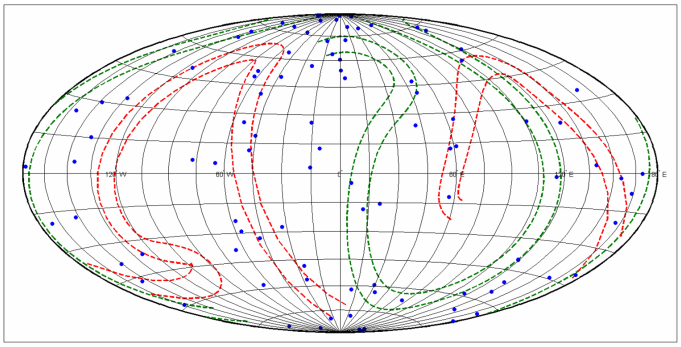

Figure 23. Skyplot of the areas of the sky which are easily accessible by two different Quasi-Halo orbits

2. Optimization of the Formation

The global optimization problem of finding each occulter's itinerary is transformed into a TSP as we did in the case of the single occulter. Then, this TSP problem is solved with the initial feed obtained in the section above, employing the same technique as the single occulter TSP. The last two procedures of initialization and TSP solving are repeated until a reasonable global solution is achieved. Figure 24 shows the optimal solution trajectory for a mission scenario consisting of two occulters and no revisiting. These results give us an approximate Delta-V budget for different configurations, which will be useful in a trade-off study of various constellations.

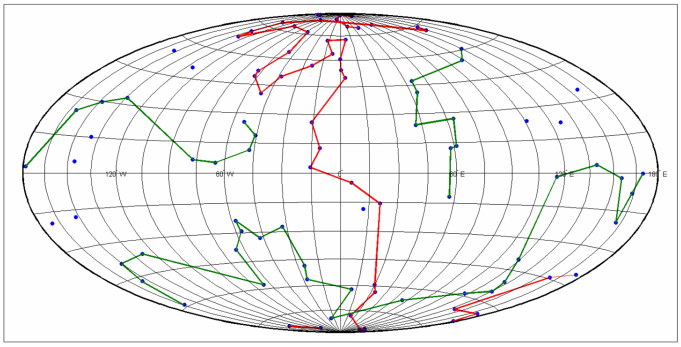

Figure 24. A possible global optimal solution to the two occulter TSP, for 90 imaging sessions of the Top 100 TPF-C stars, with 2 weeks flight time between targets and no revisiting

IV. Conclusions

A methodology to find the optimal configuration of satellite formations consisting of a telescope and multiple occulters around Sun-Earth L2 Halo orbits is outlined. Dynamics around L2 is examined with a focus on the Quasi-Halo orbits which are of interest for occulter placement. Trajectory optimization of the occulter motion between imaging sessions of different stars is performed. This enabled the transformation of the global optimization problem into a Time-Dependent TSP. First, the TSP is solved for a simpler formation consisting of a telescope and a single occulter. Using dynamical insight around L2, approximate initialization regions of the occulter formation are identified. Combining the initialization and the methods developed for single occulter formation, a solution to the full TSP is obtained. A trade-off study employing more occulters in terms of cost and scientific achievement will be completed as part of future research.

References

[1]Vanderbei, R. J., Spergel, D. N., and Kasdin, N. J., "Circularly Symmetric Apodization via Starshaped Masks," *The Astrophysical Journal*, Vol. 599, 2003, pp. 686.

[2]Vanderbei, R. J., Spergel, D. N., and Kasdin, N. J., "Spiderweb Masks for High-Contrast Imaging," *The Astrophysical Journal*, Vol. 590, 2003, pp. 593.

[3]Cash, W., "Detection of Earth-like planets around nearby stars using a petal shaped occulter," *Nature*, , No. 442, July 2006, pp. 51–53.

[4]Kolemen, E., Kasdin, N. J., and Gurfil, P., "Quasi-Periodic Orbits of the Restricted Three Body Problem Made Easy," *Proceedings of the New Trends in Astrodynamics and Applications*, August 2006.

[5]Kolemen, E. and Kasdin, N. J., "Optimal Trajectory Control of an Occulter Based Planet Finding Telescope," February 2007, AAS 07-037.

[6]Gómez, G., Masdemont, J., and Simó, C., "Quasihalo Orbits Associated with Libration Points," *Journal of The Astronautical Sciences*, Vol. 46, No. 2, 1999, pp. 1–42.

[7]Jorba, A. and Villanueva, J., "Numerical Computation of Normal Forms Around Some Periodic Orbits of the Restricted Three Body Problem," *Physica D*, Vol. 114, 1998, pp. 197–229.

[8]Jorba, A. and Masdemont, J., "Dynamics in the Center Manifold of the Restricted Three–Body Problem," *Physica D*, Vol. 132, 1999, pp. 189–213.

[9]Mattheij, R. M. M. and Staarink, G. W. M., "An efficient algorithm for solving general linear two-point BVP," *SIAM J. Sci. Stat. Comp.*, Vol. 5, 1984, pp. 87–14.

[10]Kevrekidis, I. G., Aris, R., Schmidt, L. D., and Pelikan, S., "Numerical computations of invariant circles of maps," *Physica D*, Vol. 16, 1985, pp. 243–251.

[11]Gómez, G. and Mondelo, J. M., "The dynamics around the collinear equilibrium points of the RTBP," *Physica D*, Vol. 157, No. 4, October 2001, pp. 283–321.

[12]Mondelo, J. M., *Contribution to the Study of Fourier Methods for Quasi-Periodic Functions and the Vicinity of the Collinear Libration Points*, Ph.D. thesis, Universitat de Barcelona, Departament de Matemàtica Aplicada i Anàlisi, 2001.

[13]Kierzenka, J. and Shampine, L. F., "A BVP solver based on residual control and the Maltab PSE," *ACM Trans. Math. Softw.*, Vol. 27, No. 3, 2001, pp. 299–316.

[14]Vanderbei, R. J., "LOQO: An interior point code for quadratic programming," *Optimization Methods and Software*, Vol. 11, 1999, pp. 451–484.

[15]Wächter, A. and Biegler, L. T., "Line Search Filter Methods for Nonlinear Programming: Motivation and Global Convergence," *SIAM Journal on Optimization*, Vol. 16, No. 1, 2005, pp. 1–31.

[16]`http://sco.stsci.edu/roses/index.php`, Top 100 TPF-C Targets.

[17]Glover, F. and Laguna, M., *Tabu Search*, Kluwer Academic Publishers, Norwell, MA, 1997.